

FILE COPY
NO. 2-W

N 62 57801

CASE FILE COPY

TECHNICAL MEMORANDUMS

NATIONAL ADVISORY COMMITTEE FOR AERONAUTICS

No. 801

CORRECTION OF DOWNWASH IN WIND TUNNELS
OF CIRCULAR AND ELLIPTIC SECTIONS

By Irmgard Lotz

Luftfahrtforschung
Vol. 12, No. 8, December 25, 1935
Verlag von R. Oldenbourg, Munchen und Berlin

Washington
July 1936

FILE COPY
To be returned to
the files of the National
Advisory Committee
for Aeronautics
Washington, D. C.

NATIONAL ADVISORY COMMITTEE FOR AERONAUTICS

TECHNICAL MEMORANDUM NO. 801

CORRECTION OF DOWNWASH IN WIND TUNNELS
OF CIRCULAR AND ELLIPTIC SECTIONS*

By Irmgard Lotz

SUMMARY

In this paper the downwash velocity distribution behind the wing was determined for the free jet and for the closed tunnel of both circular and elliptic cross sections. The wing was placed at the center of the tunnel. The theory makes it possible to determine the downwash at any point in the jet. The computations were performed for points in the plane determined by the jet axis and the center-of-pressure line of the wing. The elliptic tunnel section chosen had an axis ratio equal to $\sqrt{2}$. The downwash proved to be proportional to the wing lift and inversely proportional to the cross-sectional area of the tunnel. Moreover, for the circular jet the downwash depends only on the distance from the wing (see formula (29), figs. 8 and 9) and for the elliptical jet it may be approximately represented by the product of a function depending only on the ratio wing span/jet width (fig. 25 for the free jet and fig. 35 for the closed tunnel), by a function depending only on the distance from the wing (fig. 24 for the free jet and fig. 34 for the closed tunnel).

The downwash velocities induced at the wing and due to the boundary effect of the jet have been computed for jets of different cross sections. The downwash velocities in the region behind the wing have, on the contrary, received very little attention. A knowledge of these velocities in the neighborhood of the wing, especially at the position of the tail surfaces is necessary, however, for the computation of the corrected pitching moments. At the same time it may be determined whether the curvature of the flow lines is sufficiently large to explain the experimental fact that the correction factor for the angle of attack is larger than that for the drag.

* "Korrektur des Abwindes in Windkanalen mit kreisrunden oder elliptischen Querschnitten." Luftfahrtforschung, vol. 12, no. 8, December 25, 1935, pp. 250-264.

A. INTRODUCTION

Up to the present the tunnel interference effect has been determined only at the wing - more exactly, at the center of pressure of the middle wing section. The downwash velocity at this point could be simply determined since it is exactly half of the velocity with infinite flow, and the latter may be presented as a two-dimensional potential flow problem: a system of images of the trailing vortices being set up at the boundary (references 1 to 4). Figures 1 and 2 show these vortex images for open and closed circular jets. In the open tunnel the vortex images have the same sign as the original vortex; in the closed tunnel they have the opposite sign.

The values of the downwash velocities from the wing outward to infinity were not known. For a rectangular tunnel Glauert, who was interested in deriving a correction factor for the horizontal tail surface of an airplane, obtained a first approximation. For tunnels of other cross sections there was no comprehensive treatment.¹⁾ Seiferth has indeed tried to obtain better results for the circular free jet, but failed to obtain the proper correction factors even at small distances from the wing. In the present paper, in part B, will be given the exact computation of the induced velocities for circular jets, and in part C for jets of elliptical cross section.

B. JETS OF CIRCULAR CROSS SECTION

I. Statement of the Problem and Notation

To a first approximation an airfoil may be replaced by a "horseshoe vortex," which corresponds to a uniform lift distribution (fig. 3). Wings with nonuniform distribution may be replaced by several horseshoe vortices of

¹⁾ Shortly after part B of our paper was completed, there appeared the Aerodynamic Theory of W. F. Durand, vol. II, in which Burgers considers the same problem but for a circular jet only. The methods are entirely different. In the case of the free jet there is excellent agreement in the results. For the closed tunnel, however, there are certain deviations which will later be considered.

different widths $2b$ (fig. 4). We shall therefore first carry out the computations for a horseshoe vortex. We shall use the following notation: The x axis coincides with the axis of the jet, the y axis lies along the span, and the z axis is perpendicular to both and directed downward. Figure 5 shows the coordinate system used. The transverse part of the horseshoe extends from $y = -b$ to $y = +b$, the trailing vortices run parallel to the x axis from $x = 0$ to $x = -\infty$. The circulation of the vortex will be denoted by Γ . The radius of the tunnel is r_0 . We set:

$$\left. \begin{aligned} y^2 + z^2 &= r^2 = r_0^2 \rho^2 \\ \frac{y}{r_0} &= \rho \sin \varphi; \frac{z}{r_0} = \rho \cos \varphi \\ \frac{x}{r_0} &= \xi \text{ and } \frac{b}{r_0} = \kappa \end{aligned} \right\} \quad (1)$$

For infinitely extended flow the horseshoe vortex induces at the convex surface of the cylinder the tangential velocities u_0 in the direction of the x axis and v_{t_0} perpendicular to u_0 , and the normal velocity v_{n_0} .

In the case of the free jet the pressure must be constant at the jet boundaries; that is, the velocities u_0 and v_{t_0} must vanish. We must therefore superimpose a velocity field which is regular within the cylinder and on the cylinder surface has the values $-u_0$ and $-v_{t_0}$.

In the case of the closed tunnel the normal velocity v_{n_0} must vanish. The superimposed field must therefore have the velocity $-v_{n_0}$ at the boundary.

II. Determination of the Downwash for the Free Jet

We shall first consider the free jet. The boundary conditions for infinitely large $-x$ may be satisfied by introducing the images of the horseshoe vortices outside the jet as shown in figure 6. This method is known from previous investigations (Prandtl, *Tragflügeltheorie II*, p. 54). We denote the potential of the horseshoe vortex by Φ_0 , that of the image vortices by Φ_1 . The potential $(\Phi_0 + \Phi_1)$ will then satisfy the boundary conditions for

very large negative values of $\xi = x/r_0$. For finite values of ξ there still remain tangential velocities at the cylinder surface. Figure 7 shows the velocities $u_0 + u_1$ and $v_{t_0} + v_{t_1}$ plotted against φ . The function $u_0 + u_1$ is even in φ and ξ ; the function $v_{t_0} + v_{t_1}$ is uneven in φ and ξ . Both decrease rapidly with increasing $|\xi|$. To compensate these velocities, we introduce a potential Φ_2 whose derivatives $\partial\Phi_2/\partial x$ and $\partial\Phi_2/r\partial\varphi$ vanish at infinity and on the convex cylinder surface; that is, for $r = r_0$ and $\rho = 1$, assumes the values:

$$\frac{\partial\Phi_2}{\partial x} = -\frac{\partial(\Phi_0 + \Phi_1)}{\partial x}; \quad \frac{\partial\Phi_2}{r\partial\varphi} = -\frac{\partial(\Phi_0 + \Phi_1)}{r\partial\varphi} \quad (2)$$

Φ_2 must satisfy the potential equation $\Delta\Phi_2 = 0$ which, in cylindrical coordinates, reads:

$$\frac{1}{r} \frac{\partial\Phi_2}{\partial r} + \frac{\partial^2\Phi_2}{\partial r^2} + \frac{1}{r^2} \frac{\partial^2\Phi_2}{\partial\varphi^2} + \frac{\partial^2\Phi_2}{\partial x^2} = 0 \quad (3)$$

We shall first assume the function Φ_2 , instead of vanishing as $\xi = \frac{x}{r_0} \rightarrow \infty$, to be periodic in ξ . We shall then in our computations allow the period $2l = 2l^* r_0$ to increase indefinitely. The assumed series for

$$\Phi_2 = \frac{\Gamma}{4\pi} \sum_m \cos m\varphi \sum_k D_{mk} \sin\left(\frac{k\pi}{l^*}\xi\right) J_m\left(i\frac{k\pi}{l^*}\rho\right) \quad (4)$$

where D_{mk} are as yet undetermined coefficients and J_m are Bessel functions of the first kind, satisfies the differential equation, since each term of the sum satisfies it.

In order that Φ_2 may fulfill the boundary condition, it is necessary that

$$\begin{aligned} \left(\frac{\partial\Phi_2}{\partial x}\right)_{r_0} &= \frac{\Gamma}{4\pi r_0} \sum_m \cos m\varphi \sum_k D_{mk} \frac{k\pi}{l^*} \cos\left(\frac{k\pi}{l^*}\xi\right) J_m\left(i\frac{k\pi}{l^*}\right) \\ &= -\left(\frac{\partial(\Phi_0 + \Phi_1)}{\partial x}\right)_{r_0} \end{aligned} \quad (5)$$

If we now develop $\left(\frac{\partial(\Phi_0 + \Phi_1)}{\partial x}\right)_{r_0}$ (see fig. 7) into a Fourier series in φ

$$+ \left(\frac{\partial(\Phi_0 + \Phi_1)}{\partial x}\right)_{r_0} = \frac{\Gamma}{4\pi r_0} \sum_{m=1}^{\infty} l_m(\xi) \cos m\varphi \quad (5)$$

the boundary condition will read:

$$\begin{aligned} \frac{\Gamma}{4\pi r_0} \sum_m \cos m\varphi \sum_k D_{mk} \frac{k\pi}{l^*} \cos \left(\frac{k\pi}{l^*} \xi\right) J_m \left(i \frac{k\pi}{l^*}\right) \\ = - \frac{\Gamma}{4\pi r_0} \sum_m l_m(\xi) \cos m\varphi \end{aligned} \quad (5a)$$

and by comparing coefficients, we obtain:

$$\sum_k D_{mk} \frac{k\pi}{l^*} \cos \left(\frac{k\pi}{l^*} \xi\right) J_m \left(i \frac{k\pi}{l^*}\right) = - l_m(\xi) \quad (6a)$$

If we further expand the function $l_m(\xi)$ into a cosine series in ξ , $\left(\frac{\partial(\Phi_0 + \Phi_1)}{\partial x}\right)$ is an even function in ξ , we again obtain by comparison the values of the unknown coefficients

$$D_{mk} = - \frac{1}{l^*} \frac{1}{\frac{k\pi}{l^*} J_m \left(i \frac{k\pi}{l^*}\right)} \int_{-l^*}^{+l^*} l_m(\alpha) \cos \left(\frac{k\pi}{l^*} \alpha\right) d\alpha \quad (7)$$

In this way we finally obtain, by substituting (7) in (4) the expression for Φ_2

$$\Phi_2 = - \frac{\Gamma}{4\pi} \sum_m \cos m\varphi \sum_k \frac{J_m \left(\frac{ik\pi}{l^*} \rho\right) \sin \left(\frac{k\pi}{l^*} \xi\right)}{\frac{k\pi}{l^*} J_m \left(i \frac{k\pi}{l^*}\right)} \int_{-l^*}^{+l^*} l_m(\alpha) \cos \left(\frac{k\pi}{l^*} \alpha\right) d\alpha \quad (8)$$

If we now allow the period l^* to increase so that in the limit $\frac{k\pi}{l^*} = q$; $\frac{\pi}{l^*} = dq$, then the expression for the potential becomes:

$$\Phi_2 = - \frac{\Gamma}{4\pi} \sum_m \cos m\varphi \int_0^\infty \frac{\sin q\xi J_m(iq\rho)}{q J_m(iq)} dq \frac{1}{\pi} \int_{-\infty}^{+\infty} l_m(\alpha) \cos q\alpha d\alpha \quad (9)$$

In the plane of the wing (that is, to a great approximation, in the xy plane for which $\varphi = 90^\circ$ or 270°), there is obtained for the downwash velocity due to Φ_2

$$\frac{\partial \Phi_2}{\partial \varphi} = \frac{\Gamma}{4\pi r} \sum_m m \sin m\varphi \int_0^\infty \frac{\sin q\xi J_m(iq\varphi)}{q J_m(iq)} dq \frac{1}{\pi} \int_{-\infty}^{+\infty} l_m(\alpha) \cos q\alpha d\alpha \quad (10)$$

and in the symmetry line of the wing, that is, for $r = 0$

$$\frac{\partial \Phi_2}{\partial \varphi} = \pm \frac{\Gamma}{4\pi r_0} \int_0^\infty \frac{\sin q\xi \frac{1}{2} dq}{J_1(iq)} \frac{1}{\pi} \int_{-\infty}^{+\infty} l_1(\alpha) \cos q\alpha d\alpha \quad (11)$$

which is a relatively simple expression.

The potential Φ_2 was so determined that the condition:

$$\begin{aligned} \left(\frac{\partial \Phi_2}{\partial x} \right)_{r_0} &= - \left(\frac{\partial (\Phi_0 + \Phi_1)}{\partial x} \right)_{r_0} \\ &= - \frac{\Gamma}{4\pi r_0} \frac{\cos \varphi}{\xi^2 + \cos^2 \varphi} \left[-\sin \varphi \left\{ \frac{1}{\sqrt{\xi^2 + 1 + \kappa^2 - 2\kappa \sin \varphi}} - \right. \right. \\ &\quad \left. \left. \frac{1}{\sqrt{\xi^2 + 1 + \kappa^2 + 2\kappa \sin \varphi}} \right\} \right. \\ &\quad \left. + \kappa \left\{ \frac{1}{\sqrt{\xi^2 + 1 + \kappa^2 - 2\kappa \sin \varphi}} + \right. \right. \\ &\quad \left. \left. \frac{1}{\sqrt{\xi^2 + 1 + \kappa^2 + 2\kappa \sin \varphi}} \right\} \right. \\ &\quad \left. - 2 \sin \varphi \left\{ \frac{\kappa}{\sqrt{\xi^2 \kappa^2 + 1 + \kappa^2 - 2\kappa \sin \varphi}} - \right. \right. \\ &\quad \left. \left. \frac{\kappa}{\sqrt{\xi^2 \kappa^2 + 1 + \kappa^2 + 2\kappa \sin \varphi}} \right\} \right. \\ &\quad \left. + \left\{ \frac{1}{\sqrt{\xi^2 \kappa^2 + 1 + \kappa^2 - 2\kappa \sin \varphi}} + \right. \right. \\ &\quad \left. \left. \frac{1}{\sqrt{\xi^2 \kappa^2 + 1 + \kappa^2 + 2\kappa \sin \varphi}} \right\} \right] \quad (12) \end{aligned}$$

was satisfied. We must still show that the condition

$$\left(\frac{\partial \Phi_2}{\partial \varphi}\right)_{r_0} = - \left(\frac{\partial(\Phi_0 + \Phi_1)}{r \partial \varphi}\right)_{r_0} \quad (13)$$

is simultaneously satisfied.

On the surface of the cylinder the tangential velocity is

$$\left(\frac{\partial \Phi_2}{r \partial \varphi}\right)_{r_0} = \frac{\Gamma}{4\pi r_0} \sum_m m \sin m\varphi \int_0^\infty \frac{\sin q\xi}{q} dq \frac{1}{\pi} \int_{-\infty}^{+\infty} l_m(\alpha) \cos q \alpha d\alpha \quad (14)$$

This expression then must be set equal to the negative of the derivative $\left(\frac{\partial(\Phi_0 + \Phi_1)}{r \partial \varphi}\right)_{r_0}$. For the derivative,

$\left(\frac{\partial(\Phi_0 + \Phi_1)}{\partial x}\right)_{r_0}$, we assumed the expansion

$$\left(\frac{\partial(\Phi_0 + \Phi_1)}{\partial x}\right)_{r_0} = \frac{\Gamma}{4\pi r_0} \sum_m l_m(\xi, 1) \cos m\varphi \quad (\text{see equation (6)}) \quad (14a)$$

for simplicity

$$l_m(\xi, 1) \text{ was written } l_m(\xi)$$

From this it follows that the potential $(\Phi_0 + \Phi_1)$ must have the form

$$\Phi_0 + \Phi_1 = \frac{\Gamma}{4\pi} \sum_m \tau_m(\xi, \rho) \cos m\varphi \quad (15)$$

where

$$l_m(\xi, \rho) = \frac{\partial \tau_m(\xi, \rho)}{\partial \xi} \quad (16)$$

For the tangential velocity $\left(\frac{\partial(\Phi_0 + \Phi_1)}{r \partial \varphi}\right)_{r_0}$ we then obtain by differentiation of (15) the equation

$$\left(\frac{\partial(\Phi_0 + \Phi_1)}{r \partial \varphi}\right)_{r_0} = - \frac{\Gamma}{4\pi r_0} \sum_m m \tau_m(\xi, 1) \sin m\varphi \quad (17)$$

Now condition (13) requires that the derivatives (14) and (17) be equal and opposite. Since both are sine series in Φ , the coefficients of each harmonic must be equal to each other except for sign; that is, it is necessary that

$$\int_0^\infty \frac{\sin q\xi}{q} dq \frac{1}{\pi} \int_{-\infty}^{+\infty} l_m(\alpha, 1) \cos q \alpha d\alpha = + \tau_m(\xi, 1) \quad (18)$$

If we integrate the left side partially with respect to α , we obtain, using (16) the equation

$$+ \int_0^\infty \sin q \xi dq \frac{1}{\pi} \int_{-\infty}^{+\infty} \tau_m(\alpha, 1) \sin q \alpha d\alpha = \tau_m(\xi, 1) \quad (19)$$

and it is immediately seen that the left side is the Fourier representation of the function $\tau_m(\xi, 1)$; the potential Φ_2 therefore satisfies all conditions.²⁾

We shall briefly summarize what we have done so far: An airfoil in a free jet is compared with an airfoil in an infinite flow, the potential of whose disturbing field is $\Phi_1 + \Phi_2$. Due to the jet boundaries the additional downward velocities $w_k = \frac{\partial(\Phi_1 + \Phi_2)}{\partial z}$ are induced. For the plane of the wing (that is, to a close approximation, in the xy plane):

$$\frac{\partial(\Phi_1 + \Phi_2)}{\partial z} = + \frac{\partial(\Phi_1 + \Phi_2)}{r \partial \varphi} \quad (\varphi = 90^\circ \text{ to } 270^\circ) \quad (19a)$$

The derivative $\frac{\partial \Phi_2}{r \partial \varphi}$ is given by equation (10) and $\frac{\partial \Phi_1}{r \partial \varphi}$ by

2)

It may be shown that the problem of determining a potential having predetermined values for the tangential derivatives at the boundary reduces to the problem of determining a potential whose values are given at the boundary surface; that is, to a boundary problem of the first kind. For this reason, both conditions (12) and (13) are equivalent to a single condition.

$$\begin{aligned}
 -\left(\frac{\partial \Phi_1}{\partial \varphi}\right)_{\varphi=90^\circ} &= \left(\frac{\partial \Phi_1}{\partial z}\right)_{z=0} = \frac{\Gamma}{4\pi r_0} \left\{ \frac{1}{\xi} \left[2 - \frac{\rho + \frac{1}{\kappa}}{\sqrt{\xi^2 + (\rho + \frac{1}{\kappa})^2}} + \frac{\rho - \frac{1}{\kappa}}{\sqrt{\xi^2 + (\rho - \frac{1}{\kappa})^2}} \right] \right. \\
 &\quad \left. - \frac{1}{\rho - \frac{1}{\kappa}} \left(1 - \frac{\xi}{\sqrt{\xi^2 + (\rho + \frac{1}{\kappa})^2}} \right) + \frac{1}{\rho + \frac{1}{\kappa}} \left(1 - \frac{\xi}{\sqrt{\xi^2 + (\rho + \frac{1}{\kappa})^2}} \right) \right\} \tag{20}
 \end{aligned}$$

Along the tunnel axis we finally obtain (see equation (11)):

$$\begin{aligned}
 \frac{\partial(\Phi_1 + \Phi_2)}{\partial z} &= w_k = \frac{\Gamma}{4\pi r_0} \left\{ \frac{2}{\xi} \left[1 - \frac{1}{\sqrt{\xi^2 \kappa^2 + 1}} \right] + \right. \\
 &\quad \left. 2\kappa \left[1 - \frac{\xi \kappa}{\sqrt{\xi^2 \kappa^2 + 1}} \right] \right\} - \frac{\Gamma}{4\pi r_0} \int_0^\infty \frac{\sin(q\xi) \frac{i}{2} dq}{J_1(iq)} \frac{1}{\pi} \int_{-\infty}^{+\infty} l_1(a) \cos qa da \tag{21}
 \end{aligned}$$

For small values of ξ the first term simplifies to

$$\left(\frac{\partial \Phi_1}{\partial z}\right)_{z=0, y=0} = \frac{\Gamma}{4\pi r_0} (2\kappa - \kappa^2 \xi) \tag{21a}$$

The downward induced velocities along the axis for different ratios of wing span to jet diameter are determined from equation (21). (See section IV.)

III. Determination of the Induced Downward Velocities for the Closed Tunnel

A similar procedure is applied to closed tunnels. Images of the horseshoe vortices are first introduced with the sign of the circulation changed. (Fig. 2 shows a section through the tunnel at a great distance from the wing.) Then the superimposed potential Φ_2^* is determined in a similar way as was done for the open channel. We thus obtain

$$\Phi_2^* = -\frac{\Gamma}{4\pi} \sum_m \cos m\varphi \int_0^\infty \frac{J_m(iq\varphi) \sin q\xi dq}{iq J_m'(iq)} \frac{1}{\pi} \int_{-\infty}^{+\infty} g_m(\alpha, l) \sin q\alpha d\alpha \quad (22)$$

in which J_m' is the derivative of the Bessel function of the first kind and m th order.

The functions g_m are so determined that

$$\begin{aligned} \left(\frac{\partial \Phi_2^*}{\partial r} \right)_{r_0} &= - \left(\frac{\partial (\Phi_0 + \Phi_1)}{\partial r} \right)_{r_0} \\ &= - \frac{\Gamma}{4\pi r_0} \left\{ \kappa \cos \varphi \left[\frac{1}{1+\kappa^2-2\kappa \sin \varphi} \left(\frac{\xi \kappa}{\sqrt{\xi^2 \kappa^2 + 1 + \kappa^2 - 2\kappa \sin \varphi}} \right. \right. \right. \\ &\quad \left. \left. \left. - \frac{\xi}{\sqrt{\xi^2 + 1 + \kappa^2 - 2\kappa \sin \varphi}} \right) \right. \right. \\ &\quad \left. \left. + \frac{1}{1+\kappa^2+2\kappa \sin \varphi} \left(\frac{\xi \kappa}{\sqrt{\xi^2 \kappa^2 + 1 + \kappa^2 + 2\kappa \sin \varphi}} \right. \right. \right. \\ &\quad \left. \left. \left. - \frac{\xi}{\sqrt{\xi^2 + 1 + \kappa^2 + 2\kappa \sin \varphi}} \right) \right] \right. \\ &\quad \left. - \frac{\xi \cos \varphi}{\xi^2 + \cos^2 \varphi} \left[2 + \sin \varphi \left(\frac{\kappa}{\sqrt{\xi^2 \kappa^2 + 1 + \kappa^2 - 2\kappa \sin \varphi}} \right. \right. \right. \\ &\quad \left. \left. \left. - \frac{\kappa}{\sqrt{\xi^2 \kappa^2 + 1 + \kappa^2 + 2\kappa \sin \varphi}} \right) \right] \right. \\ &\quad \left. - \left(\frac{1}{\sqrt{\xi^2 \kappa^2 + 1 + \kappa^2 - 2\kappa \sin \varphi}} + \frac{1}{\sqrt{\xi^2 \kappa^2 + 1 + \kappa^2 + 2\kappa \sin \varphi}} \right) \right. \\ &\quad \left. + \sin \varphi \left(\frac{1}{\sqrt{\xi^2 + 1 + \kappa^2 + 2\kappa \sin \varphi}} - \frac{1}{\sqrt{\xi^2 + 1 + \kappa^2 - 2\kappa \sin \varphi}} \right) \right. \\ &\quad \left. + \kappa \left(\frac{1}{\sqrt{\xi^2 + 1 + \kappa^2 + 2\kappa \sin \varphi}} + \frac{1}{\sqrt{\xi^2 + 1 + \kappa^2 - 2\kappa \sin \varphi}} \right) \right] \right\} \\ &= - \frac{\Gamma}{4\pi r_0} \sum_m g_m(\xi, l) \cos m\varphi \quad (23) \end{aligned}$$

The induced velocity, arising from the tunnel boundary effect, in the plane $z = 0$, is

$$\begin{aligned}
 w_k^* = & - \frac{\Gamma}{4\pi r_0} \left\{ \frac{1}{\xi} \left[2 - \frac{\rho + \frac{1}{\kappa}}{\sqrt{\xi^2 + (\rho + \frac{1}{\kappa})^2}} + \frac{\rho - \frac{1}{\kappa}}{\sqrt{\xi^2 + (\rho - \frac{1}{\kappa})^2}} \right] \right. \\
 & - \left. \frac{1}{\rho - \frac{1}{\kappa}} \left(1 - \frac{\xi}{\sqrt{\xi^2 + (\rho - \frac{1}{\kappa})^2}} \right) + \frac{1}{\rho + \frac{1}{\kappa}} \left(1 - \frac{\xi}{\sqrt{\xi^2 + (\rho + \frac{1}{\kappa})^2}} \right) \right\} \\
 & - \frac{\Gamma}{4\pi r} \sum_m m \sin m \varphi \int_0^\infty \frac{J_m(iq\rho) \sin q \xi dq}{i q J_m'(iq)} \frac{1}{\pi} \int_{-\infty}^{+\infty} g_m(\alpha, 1) \sin q \alpha d\alpha
 \end{aligned} \tag{24}$$

and for the line of symmetry $y = 0$:

$$\begin{aligned}
 w_k^* = & - \frac{\Gamma}{4\pi r_0} \left\{ \frac{2}{\xi} \left[1 - \frac{1}{\sqrt{\xi^2 \kappa^2 + 1}} \right] + 2\kappa \left[1 - \frac{\xi \kappa}{\sqrt{\xi^2 \kappa^2 + 1}} \right] \right\} \\
 & - \frac{\Gamma}{4\pi r_0} \int_0^\infty \frac{\frac{1}{2} \sin q \xi dq}{J_1'(iq)} \frac{1}{\pi} \int_{-\infty}^{+\infty} g_m(\alpha, 1) \sin q \alpha d\alpha
 \end{aligned} \tag{25}$$

From equation (25) are computed the induced velocities for various ratios of wing span to tunnel diameter. (See section IV.)

IV. Numerical Results

Sections II and III supply the theoretical basis for the computation of the induced velocities due to boundary effect. These velocities w_k and w_k^* are computed from equations (21) and (25) for any point on the axis of the wind tunnel.

When the blower velocity is V the change in the flow direction at each point is w_k/V . The induced velocity at the wing will be denoted by w_{k_0} . The correction for the angle of attack of the wing itself is then

$$\alpha_k = \frac{w_{k_0}}{V} = \frac{\Gamma}{4\pi r_0 V} 2\kappa$$

$$\left(\Gamma = \text{circulation}, \kappa = \frac{2b}{2r_0} = \frac{\text{wing span}}{\text{tunnel diameter}} \right)$$

or, substituting the lift coefficient c_a

$$\alpha_k = \frac{w_{k_0}}{V} = \frac{1}{8} \frac{F}{F_0} c_a \quad (26)$$

(F = area of wing, F_0 = cross-sectional area of jet).

At a distance l from the wing the effect of the tunnel boundary on the downwash is larger than at the wing itself. The tail surfaces in that position would therefore have a different effect on the pitching moment than would be the case in free flight. In the free jet the effective angle of attack is reduced by the amount

$$\beta_k = \frac{w_k - w_{k_0}}{V} \quad (27)$$

in the closed tunnel it is increased by the amount

$$\beta_k^* = \frac{w_k^* - w_{k_0}^*}{V} \quad (28)$$

The upwash at the wing in the closed tunnel is numerically equal to the downwash of the same wing in the free jet, $w_{k_0}^* = -w_{k_0}$.

Figure 8 shows the ratio $\tau = \beta_k/\alpha_k$ plotted against $l/2r_0$ for the free jet. Figure 9 shows the similar relations for the closed jet.³⁾ The computations showed that the quotients τ and τ^* are practically independent of the ratio span/tunnel diameter. Since any distribution whatever could be built up by superposition of uniform

3) Contrary to what was found by Burgers (reference 5) τ^* for the closed tunnel approaches the asymptote from above. W. L. Cowley and G. A. McMillan (reference 6) have recently improved the Glauert computation for the rectangular tunnel and have also shown that τ^* approaches the asymptote from above (for ratios of span to tunnel diameter less than 0.55). The x_4 curve there given would be similar for the case of a square tunnel but have its maximum at $x/b = 1$ (b = width of tunnel).

distributions along spans of different lengths, the results are also independent of the lift distribution. For the free jet, higher values are obtained than those obtained by the Seiferth approximation.

The induced velocity itself instead of the change in angle of attack, may easily be determined from the curves (figs. 8 and 9):

$$\left. \begin{aligned} w_k &= \frac{1}{8} \frac{F}{F_0} c_a (1 + \tau) v \\ w_k^* &= - \frac{1}{8} \frac{F}{F_0} c_a (1 + \tau^*) v \end{aligned} \right\} \quad (29)$$

It should be noted that by the above theory it is possible to compute the downwash at every point in the wind tunnel. Thus, for example, for a ratio of wing span/free-jet diameter = 0.45, the downwash was computed all along a parallel to the tunnel axis in the xy plane (fig. 5) passing through the wing tip. The values differ by an insignificant amount from those along the tunnel axis.

The downwash resulting from the jet boundary produces a curvature of the flow. We shall now investigate whether this curvature is sufficient to explain the experimental fact that the correction factor for the angle of attack is larger than the drag correction factor.

Since, along the wing chord, the curves τ and τ^* (see equation (29) and figs. 8 and 9) may be replaced by their tangents $f'(0)$ and $f^{*'}(0)$ through the origin, the downwash may be given by the expression

$$w_k = w_{k_0} \left[1 + f'(0) \frac{l}{2r_0} \right] \quad (30)$$

The curvature of the streamlines at the wing is therefore

$$\frac{1}{R} = \frac{f'(0)}{2r_0} \frac{w_{k_0}}{v} \quad (31)$$

where $f'(0) = 1.58$ for the free jet and $f^{*'}(0) = 2.1$ for the closed tunnel.

It is customary to write the correction for the angle of attack due to the boundary effect in the form

$$\alpha_k = \frac{\delta}{8} \frac{F}{F_0} c_a$$

For circular tunnels $\delta = \pm 1$. This factor is computed on the assumption that the wing is replaced by a lift line. Since the wing, however, has finite chord, the jet curvature does affect its camber characteristics. In a free jet the camber is decreased - that is, the effective angle of attack is decreased; in a closed tunnel it is increased, and therefore the effective angle of attack is increased. Seiferth (reference 1) investigated the effect of jet curvature on a profile having the form of an arc of a circle. If t denotes the profile chord, then the change in the angle of attack of a wing section due to the streamline curvature is of the amount

$$\Delta \alpha = \frac{t}{4R} \quad (32)$$

If we substitute the value for R given by equation (31) we obtain for the angle of attack the correction

$$\Delta \alpha = \frac{t}{2r_0} \frac{f'(0)}{4} \frac{w_{k_0}}{V} = \frac{t}{2r_0} \frac{f'(0)}{4} \alpha_k \quad (33)$$

The total correction for the angle of attack for a free jet is then

$$\begin{aligned} \alpha_k + \Delta \alpha &= \alpha_k \left[1 + \left(\frac{t}{2b} \right) \left(\frac{2b}{2r_0} \right) \frac{f'(0)}{4} \right] \\ &= \frac{1}{8} \frac{F}{F_0} c_a \left[1 + \left(\frac{t}{2b} \right) \left(\frac{2b}{2r_0} \right) \frac{f'(0)}{4} \right] \end{aligned} \quad (34)$$

that is, the factor $|\delta|$ increases by

$$100 \left(\frac{t}{2b} \right) \left(\frac{2b}{2r_0} \right) \frac{f'(0)}{4} \text{ percent} \quad (35)$$

If we compare this result with those of Knight and Harris (reference 7), there is found to be satisfactory agreement for the ratios wing span/tunnel diameter = 0.45 and 0.6; for larger ratios of $\kappa = 2b/2r_0$, the values obtained are too small. We must consider, however, that our computation was made only for the tunnel axis, so that no account was taken of the variation along the span. For large spans, for example, $\kappa = 2b/2r_0 = 0.8$, this variation along the span would increase the factor δ by 9 percent even if no account were taken of the curvature of the jet. Moreover, the test results were obtained by ex-

trapolation to infinitely large ratio of jet area to wing area and are therefore not very accurate.

C. JETS OF ELLIPTIC CROSS SECTION

I. Statement of the Problem and Notation

Due to the fact that they make the testing of large models more convenient, free jets of elliptic cross section are now preferred to circular jets. For uniform lift distribution, the induced velocities at the wing arising from the boundary effect were computed by Sanuki and Tani; Rosenhead made the computation for elliptical lift distribution (references 3 and 4). We shall determine the induced velocities behind the wing in the same way as was done for the circular jet.

We again first replace the airfoil by a horseshoe vortex, since nonuniform lift distributions may be built up by a combination of horseshoe vortices.

The direction of the coordinate axes and the notation for the various magnitudes of the horseshoe vortex are the same as in section B. The elliptic jet has its large axis equal to $2a$ and its small axis to $2b_1$. (See fig. 10.) The eccentricity is denoted by c ($c = \sqrt{a^2 - b_1^2}$). With infinite flow there are induced at the convex surface of the elliptical cylinder the tangential velocities u_0 in the direction of the x axis and v_{t_0} perpendicular to u_0 , and the normal velocity v_{n_0} .

In the case of the free jet the pressure must be constant at the jet boundary; that is, the velocities u_0 and v_{t_0} must be made to vanish. We must therefore superimpose a velocity field that is regular within the elliptic cylinder and on the boundary has the values $-u_0$ and $-v_{t_0}$.

For the closed tunnel it is necessary that the normal velocity v_{n_0} vanish. The superimposed velocity field must therefore have the value $-v_{n_0}$ on the surface of the elliptic cylinder.

II. Downwash in the Free Jet

1. Theoretical considerations.— We shall proceed in a similar manner as for the circular free jet. In that case we first set up the images of the horseshoe vortex at the cylindrical boundary and were thus enabled to satisfy the boundary condition for infinitely large negative values of x . In the case of the elliptical jet, we must similarly arrange a system of vortex filaments so that the boundary condition at infinity may be satisfied. Since the velocity u_0 approaches zero at infinity whereas the other component of the tangential velocity v_{t_0} remains finite, it is necessary to determine the vortex filaments outside the cylinder in such a manner that they make v_{t_0} vanish at infinity.

If we consider a section of the jet at an infinite distance behind the wing (fig. 11), we have an ellipse with two single vortices. We must now set up a system of vortices in the space outside the ellipse in such a manner that the velocity induced by these vortices and by the vortex pair within the ellipse is always normal to the boundary. To determine the position of these vortices we transform the ellipse into a rectangle. In figure 12 B and B' , denote the foci of the ellipse. Let there be a vortex at P_1 . By means of the function

$$y + iz = c \cosh(\eta + i\zeta) \quad (36)$$

the ellipse is transformed into a rectangle (hatched area in fig. 13). The segment $BC = a$ goes over into segment $B^*C^* = \eta_0$ on the η axis. The upper half of the ellipse is transformed into the rectangle $B^*C^*C'^*B'^*$ lying above the η axis; the lower half into the rectangle $B^*C^*C'^*B'^*$ lying below the η axis. The side of the rectangle $C'^*D^*C^*D'^*$ corresponds to the boundary of the ellipse. In order that only normal velocities arise at the boundary $C'^*D^*C^*D'^*$ and that the flow in the yz plane pass through $C'B'AB$ without disturbance, it is necessary to form images as indicated in figure 13. Let the complex coordinate of the point P_1^* be μ_1 . The image vortices then lie at

$$\begin{aligned}
 1) \quad & \mu_1 + i2n\pi + 4m\eta_0 \\
 2) \quad & (2\eta_0 - \bar{\mu}_1) + i2n\pi + 4m\eta_0 \\
 3) \quad & -\mu_1 + i2n\pi + 4m\eta_0 \\
 4) \quad & (2\eta_0 + \bar{\mu}_1) + i2n\pi + 4m\eta_0
 \end{aligned} \quad (37)$$

where $\bar{\mu}_1$ denotes the conjugate of μ_1 . Assuming that $P_1^* = \mu_1$ denotes the position of one trailing part of the horseshoe vortex, the other vortex will lie at point P_2^* whose coordinate is $\mu_2 = i\pi + \bar{\mu}_1$. The position of the corresponding image vortex may be found with the aid of equations (37) by substituting $i\pi + \bar{\mu}_1$ for μ_1 and $-i\pi + \bar{\mu}_1$ for $\bar{\mu}_1$.

In what follows we shall consider only the case where the airfoil lies in the xy plane; then the z coordinate of the trailing vortex is zero. If the span $2b$ is now greater or equal to the distance between the foci, then in the $\eta\xi$ plane all vortices will lie on the straight lines $\xi = n\pi$; if the span $2b$ is smaller than the distance between foci, the vortices will lie on the straight lines $\eta = 2m\eta_0$, where m and n run through the whole range of integers from $-\infty$ to $+\infty$. We must still determine the position of these vortices in the yz plane. Since $y = c \cosh \eta \cos \xi$ and $z = c \sinh \eta \sin \xi$ (see equation (36)), all vortices will lie on the y axis for the range $2b \geq 2c$, as $\xi = n\pi$; and for $2b < 2c$, all vortices will lie on lines for which $\xi = \text{constant} \neq n\pi$; that is, on confocal hyperbolae. As $2b$ approaches zero, all vortices lie on the z axis. Thus we have determined the positions the vortex filaments outside the boundary must have in order to satisfy the boundary condition for $x \rightarrow -\infty$.

Now let Φ_0 be the potential of the horseshoe vortex, Φ_1 the potential of the vortex filaments in the outer space. Figure 14 shows the vortex images for the case where the span is equal to or greater than the distance between foci. The figures indicated in the diagram are to be used later for working out an example. In the zy plane it is necessary to prolong the vortex filaments in some manner since a vortex filament must have no free ends and since, moreover, they cannot be prolonged parallel to the x axis because in that case the boundary condition for $x \rightarrow +\infty$ would be impossible of fulfillment. For the case

where the span is smaller than the distance between foci, the position of the vortex filaments will be as shown in figure 15. In this case it is simpler to unite the filaments rather than prolong them. This combining of the filaments would have been impossible in the first case since the transverse part would have cut the ellipse and so would not have lain in the outside region. In the case of infinitely small spans vortex pairs are obtained in the space outside the elliptic jet (fig. 16).

The potential $(\Phi_0 + \Phi_1)$ satisfies the boundary condition at infinity. In order to reduce to zero the velocities still remaining $(u_0 + u_1)$ and $(v_{t_0} + v_{t_1})$, it is necessary to superimpose a potential Φ_2 . Since Φ_2 must satisfy the above conditions on the surface of the elliptic cylinder, we introduce elliptical coordinates for greater convenience in treating the problem:

$$\left. \begin{aligned} x &= \xi \\ y &= c \cosh \eta \cos \xi \\ z &= c \sinh \eta \sin \xi \end{aligned} \right\} \quad (38)$$

In any plane $x = \text{constant}$ the curves $\eta = \text{constant}$ represent confocal ellipses and the curves $\xi = \text{constant}$, confocal hyperbolae. On the cylinder surface $\eta = \text{constant} = \eta_0$. The potential equation which Φ_2 must satisfy then reads, in elliptical coordinates:

$$\frac{\partial^2 \Phi_2}{\partial \xi^2} + \frac{1}{c^2 (\cosh^2 \eta - \cos^2 \xi)} \left(\frac{\partial^2 \Phi_2}{\partial \eta^2} + \frac{\partial^2 \Phi_2}{\partial \xi^2} \right) = 0 \quad (39)$$

In addition, the boundary conditions require that

$$\left(\frac{\partial \Phi_2}{\partial \xi} \right)_{\eta_0} = - \left(\frac{\partial (\Phi_0 + \Phi_1)}{\partial \xi} \right)_{\eta_0} \quad (40)$$

and

$$\left(\frac{\partial \Phi_2}{\partial \xi} \right)_{\eta_0} = - \left(\frac{\partial (\Phi_0 + \Phi_1)}{\partial \xi} \right)_{\eta_0} \quad (41)$$

Instead of allowing Φ_2 to vanish $\xi \rightarrow \pm \infty$, we shall first set up Φ_2 as a periodic function in ξ and then in our computation allow the period $2l = 2l^* a$ to

grow indefinitely. To solve the differential equation (39), we assume the product:

$$\Phi_2 = - \frac{\Gamma}{4\pi} \sum_v \sum_k C_{v,k} \sin \left(\frac{k\pi}{l} \xi \right) M_{v,k}(\xi) \bar{M}_{v,k}(\eta) \quad (42)$$

The function M depends only on ξ , the function \bar{M} only on η . Substituting one member of the above equation in differential equation (39),

$$- \frac{k^2 \pi^2}{l^2} \sin \left(\frac{k\pi}{l} \xi \right) M_{v,k} \bar{M}_{v,k} + \frac{1}{c^2 (\cosh^2 \eta - \cos^2 \xi)} \sin \left(\frac{k\pi}{l} \xi \right) \left(\frac{d^2 M_{v,k}(\xi)}{d\xi^2} \bar{M}_{v,k}(\eta) + \frac{d^2 \bar{M}_{v,k}(\eta)}{d\eta^2} M_{v,k}(\xi) \right) = 0 \quad (42a)$$

it is seen which equation the functions M and \bar{M} must satisfy:

$$\begin{aligned} & \frac{d^2 M_{v,k}(\xi)}{d\xi^2} \bar{M}_{v,k}(\eta) + \frac{d^2 \bar{M}_{v,k}(\eta)}{d\eta^2} M_{v,k}(\xi) \\ &= \frac{k^2 \pi^2}{l^2} c^2 (\cosh^2 \eta - \cos^2 \xi) M_{v,k}(\xi) \bar{M}_{v,k}(\eta) \\ &= \frac{k^2 \pi^2}{l^2} \frac{c^2}{2} (\cosh 2\eta - \cos 2\xi) M_{v,k}(\xi) \bar{M}_{v,k}(\eta) \end{aligned} \quad (42b)$$

Changing the order of the terms and dividing through by $M \bar{M}$, we obtain:

$$\begin{aligned} & \frac{d^2 M_{v,k}(\xi)}{d\xi^2} \frac{1}{M_{v,k}(\xi)} + \frac{k^2 \pi^2}{l^2} \frac{c^2}{2} \cos 2\xi \\ &= - \frac{d^2 \bar{M}_{v,k}(\eta)}{d\eta^2} \frac{1}{\bar{M}_{v,k}(\eta)} + \frac{k^2 \pi^2}{l^2} \frac{c^2}{2} \cosh 2\eta \end{aligned} \quad (42c)$$

Since one side depends only on the variable ξ and the other side only on η , the equality of the two sides means that they are constant. We denote the constant by $-v$, and thus obtain the equations:

$$\frac{d^2 M_{v,k}(\xi)}{d\xi^2} + \left(\frac{k^2 \pi^2}{l^2} \frac{c^2}{2} \cos 2\xi + v \right) M_{v,k}(\xi) = 0 \quad (43)$$

$$\frac{d^2 \bar{M}_{v,k}(\eta)}{d\eta^2} - \left(\frac{k^2 \pi^2}{l^2} \frac{c^2}{2} \cosh 2\eta + v \right) \bar{M}_{v,k}(\eta) = 0 \quad (44)$$

If $\eta = i\tau$ is substituted in the second equation, it assumes the same form as the first. The solutions of the first equation for real values of ξ are therefore, on substitution of a pure imaginary variable, solutions of the second. These differential equations were first investigated by Mathieu, and their solutions are known as Mathieu functions (references 8 and 9). For our problem we need consider only such Mathieu functions as are periodic in ξ . Periodic solutions, however, occur only when there exist definite relationships between the parameter v and $\frac{k^2 \pi^2}{l^2} \frac{c^2}{2}$, so that v is determined when $\frac{k^2 \pi^2}{l^2} \frac{c^2}{2}$ is given.

In addition to satisfying the differential equation, the potential Φ_2 must also satisfy the boundary conditions (40) and (41). Now the problem of determining a potential that should have given tangential derivatives at the boundary, is equivalent to the problem of determining a potential having pre-assigned values on the boundary; that is, to a boundary problem of the first kind. Therefore, both conditions (40) and (41) are equivalent to one single condition and it is therefore sufficient that the condition:

$$\left(\frac{\partial \Phi_2}{\partial \xi} \right)_{\eta_0} = - \left(\frac{\partial (\Phi_0 + \Phi_1)}{\partial \xi} \right)_{\eta_0} = - \frac{\Gamma}{4\pi a} F(\xi, \eta_0, \zeta) \quad (45)$$

is satisfied, and therefore also

$$\begin{aligned} \left(\frac{\partial \Phi_2}{\partial \xi} \right)_{\eta_0} &= - \frac{\Gamma}{4\pi} \sum_v \sum_k C_{v,k} \frac{k\pi}{l^* a} \cos \left(\frac{k\pi}{l^* a} \xi \right) \bar{M}_{v,k}(\xi) M_{v,k}(\eta_0) \\ &= - \frac{\Gamma}{4\pi a} F(\xi, \eta_0, \zeta) \end{aligned} \quad (46)$$

The constants $C_{v,k}$ must be so determined that the bound-

ary condition (46) is satisfied. Since the Mathieu functions $M_{v,k}(\xi)$ form an orthogonal system, similar to the harmonic functions, to which they reduce when the eccentricity of the ellipse approaches zero, the following relations hold true:

$$\left. \begin{aligned} \int_0^{2\pi} M_{v_n,k}(\xi) M_{v_m,k}(\xi) d\xi &= 0 \quad \text{for } n \neq m \\ \int_0^{2\pi} M^2 v_{n,k}(\xi) d\xi &= \pi \quad \text{for } n > 0 \\ \text{and } \int_0^{2\pi} M^2 v_{0,k}(\xi) d\xi &= 2\pi \end{aligned} \right\} \quad (47)$$

We shall therefore multiply equation (46) by a Mathieu function $M_{v,k}(\xi)$ and integrate over the region $0 \leq \xi \leq 2\pi$.

$$\begin{aligned} -\frac{\Gamma}{4\pi} \sum_k C_{v,k} \frac{k\pi}{l^* a} \cos\left(\frac{k\pi}{l^* a} \xi\right) \bar{M}_{v,k}(\eta_0) \\ = -\frac{\Gamma}{4\pi a} \frac{1}{\pi} \int_0^{2\pi} F(\xi, \eta_0, \xi) M_{v,k}(\xi) d\xi \end{aligned} \quad (47a)$$

which, divided by $\frac{\Gamma}{4\pi a}$, gives:

$$\begin{aligned} \sum_k C_{v,k} \frac{k\pi}{l^*} \cos\left(\frac{k\pi}{l^* a} \xi\right) \bar{M}_{v,k}(\eta_0) \\ = \frac{1}{\pi} \int_0^{2\pi} F(\xi, \eta_0, \xi) M_{v,k}(\xi) d\xi \end{aligned} \quad (47b)$$

We shall now make use of the orthogonal properties of the trigonometric functions by multiplying the equation by $\cos\left(\frac{k\pi}{l^* a} \xi\right)$ and, integrating over the region $-l^* \leq \xi \leq +l^*$. We thus obtain:

$$\begin{aligned} C_{v,k} \frac{k\pi}{l^*} \bar{M}_{v,k}(\eta_0) &= \\ \frac{1}{l^*} \int_{-l^*}^{+l^*} [\cos\left(\frac{k\pi}{l^* a} \xi\right) \frac{1}{\pi} \int_0^{2\pi} F(\xi, \eta_0, \xi) M_{v,k}(\xi) d\xi] d\left(\frac{\xi}{a}\right) \end{aligned} \quad (47c)$$

or, $c_{v,k} =$

$$\frac{1}{\frac{k\pi}{l^*} \bar{M}_{v,k}(\eta_0)} \frac{1}{l^*} \int_{-l^*}^{+l^*} [\cos\left(\frac{k\pi}{l^*} \frac{\xi}{a}\right) \frac{1}{\pi} \int_0^{2\pi} F(\xi, \eta_0, \zeta) M_{v,k}(\zeta) d\zeta] d\left(\frac{\xi}{a}\right) \quad (48)$$

Substituting these coefficients into equation (42) and setting $\frac{\xi}{a} = \alpha$ and $\zeta = \zeta^*$ under the integral signs to avoid confusion, there results for the potential Φ_2 the expression:

$$\begin{aligned} \Phi_2 = & - \frac{\Gamma}{4\pi} \sum_v \sum_k \frac{\sin\left(\frac{k\pi}{l^*} \frac{\xi}{a}\right)}{\frac{k\pi}{l^*} \bar{M}_{v,k}(\eta_0)} \\ & \frac{1}{l^*} \int_{-l^*}^{+l^*} [\cos\left(\frac{k\pi}{l^*} \alpha\right) d\alpha \frac{1}{\pi} \int_0^{2\pi} F(\alpha, \eta_0, \zeta^*) M_{v,k}(\zeta^*) d\zeta^*] \\ & M_{v,k}(\xi) \bar{M}_{v,k}(\eta) \end{aligned} \quad (49)$$

We now allow the period l^* to increase so that in the limit $\frac{k\pi}{l^*} = q$, $\frac{\pi}{l^*} = dq$, and thus obtain for the potential the final expression:

$$\begin{aligned} \Phi_2 = & - \frac{\Gamma}{4\pi} \sum_v \\ & \frac{1}{\pi} \int_0^\infty \frac{\sin\left(q \frac{\xi}{a}\right)}{q \bar{M}_{v,q}(\eta_0)} \int_{-\infty}^{+\infty} \cos q \alpha d\alpha \frac{1}{\pi} \int_0^{2\pi} F(\alpha, \eta_0, \zeta^*) M_{v,q}(\zeta^*) d\zeta^* \\ & M_{v,q}(\xi) \bar{M}_{v,q}(\eta) dq \end{aligned} \quad (50)$$

The Mathieu functions (see (43) and (44)) will then satisfy the differential equations:

$$\frac{d^2 M_{v,q}(\zeta)}{d\zeta^2} + \left(q^2 \frac{c^2}{2a^2} \cos 2\zeta + v\right) M_{v,q}(\zeta) = 0 \quad (51)$$

and

$$\frac{d^2 \bar{M}_{v,q}(\eta)}{d\eta^2} - (q^2 \frac{c^2}{2a^2} \cosh 2\eta + v) \bar{M}_{v,q}(\eta) = 0 \quad (52)$$

The downwash velocity required is now given by

$$\begin{aligned} \frac{\partial \Phi}{\partial z} = \frac{\partial \Phi_1}{\partial z} + \frac{\partial \Phi_2}{\partial z} &= \frac{\partial \Phi_1}{\partial z} + \frac{\cosh \eta \sin \zeta}{c(\cosh^2 \eta - \cos^2 \zeta)} \frac{\partial \Phi_2}{\partial \eta} \\ &+ \frac{\sinh \eta \cos \zeta}{c(\cosh^2 \eta - \cos^2 \zeta)} \frac{\partial \Phi_2}{\partial \zeta} \end{aligned} \quad (53)$$

For points in the xy plane where the y coordinate is smaller than the distance from the foci to the origin, that is, $-c \leq y \leq +c$ so that $\eta = 0$,

$$\frac{\partial \Phi}{\partial z} = \frac{\partial \Phi_1}{\partial z} + \frac{1}{c \sin \zeta} \frac{\partial \Phi_2}{\partial \eta} \quad (54)$$

and for points whose y coordinate is greater than this distance, that is, $-c \geq y \geq +c$ so that $\zeta = 0$

$$\frac{\partial \Phi}{\partial z} = \frac{\partial \Phi_1}{\partial z} + \frac{1}{c \sinh \eta} \frac{\partial \Phi_2}{\partial \zeta} \quad (55)$$

2. Numerical example. - An elliptical jet section was chosen with axis ratio⁴⁾ $a/b_1 = \sqrt{2}$. On the jet boundary the elliptic coordinate η has the value η_0 given by the relation:

$$\frac{a}{b_1} = \coth \eta_0 = \sqrt{2} \quad (55a)$$

The computations were carried out for the two following cases:

- 1) Wing span equal to the distance between foci.
- 2) Very small wing spans.

We first require the tangential velocity $\frac{\partial(\Phi_0 + \Phi_1)}{\partial \xi}$.

For the first case the vortex filaments outside the jet

⁴⁾ The notation b_1 was used for the minor axis of the ellipse to avoid confusion with the wing span.

all lie in the xy plane. The velocity at the jet boundary ($\eta = \eta_0$) is therefore,

$$\begin{aligned} \frac{\partial(\Phi_0 + \Phi_1)}{\partial \xi} &= \frac{\Gamma}{4\pi a} \frac{\frac{b_1}{a} \sin \zeta}{\left(\frac{\xi}{a}\right)^2 + \left(\frac{b_1}{a}\right)^2 \sin^2 \zeta} \\ &\left\{ \frac{\cos \zeta + \frac{b}{a}}{\sqrt{\left(\frac{\xi}{a}\right)^2 + \left(\frac{b_1}{a}\right)^2 \sin^2 \zeta + \left(\cos \zeta + \frac{b}{a}\right)^2}} - \right. \\ &\quad \frac{\cos \zeta - \frac{b}{a}}{\sqrt{\left(\frac{\xi}{a}\right)^2 + \left(\frac{b_1}{a}\right)^2 \sin^2 \zeta + \left(\cos \zeta - \frac{b}{a}\right)^2}} \\ &+ 2 \sum_{n=1}^{n=\infty} \left[-2 + \frac{\cos \zeta + d_n}{\sqrt{\left(\frac{\xi}{a}\right)^2 + \left(\frac{b_1}{a}\right)^2 \sin^2 \zeta (\cos \zeta + d_n)^2}} \right. \\ &\quad \left. \left. \frac{\cos \zeta - d_n}{\sqrt{\left(\frac{\xi}{a}\right)^2 + \left(\frac{b_1}{a}\right)^2 \sin^2 \zeta + (\cos \zeta - d_n)^2}} \right] \right\} \quad (56) \end{aligned}$$

where

$$d_n = \frac{\cosh 2n \eta_0}{\cosh \eta_0}; \quad n = 1, 2, 3 \dots \quad (56a)$$

For the second case we have pairs of vortices in the xz plane (see fig. 16); the velocity at the jet boundary is given by

$$\frac{\partial(\Phi_0 + \Phi_1)}{\partial \xi} = \frac{\Gamma 2b}{4\pi a^2} \sum_{n=-\infty}^{n=\infty} \frac{\left[\frac{b_1}{a} \sin \zeta - f_n\right] \cosh 2n \eta_0}{\sqrt{\left(\frac{\xi}{a}\right)^2 + \cos^2 \zeta + \left(\frac{b_1}{a} \sin \zeta - f_n\right)^2}} \quad (57)$$

where

$$f_n = \frac{\sinh 2n \eta_0}{\cosh \eta_0}; \quad n = 0, 1, 2, 3 \dots \quad (57a)$$

The effect of the vortex filaments lying outside the jet decreases with increasing distance from the jet. It is sufficient for practical purposes to consider, out of the infinite number of vortex filaments lying outside the jet, only the first three.

The velocity on the ξ direction is an uneven function of ξ . We must choose the corresponding Mathieu functions $M_{v,q}(\xi)$ to satisfy the differential equation (51). S. Goldstein (9) has computed several Mathieu functions using a notation for the constants different from ours. To avoid confusion, we shall employ the index G with the Goldstein parameter:

$$q^2 \frac{c^2}{2a^2} = -16 q_G; \quad v = 4\alpha_G \quad (58)$$

The uneven periodic Mathieu functions Goldstein denotes by $s e_{2n+1}(\xi)$ since they reduce to the harmonic functions $\sin(2n+1)\xi$ when the eccentricity of the ellipse approaches zero.

The Mathieu functions may be developed into Fourier series:

$$s e_{2n+1}(\xi) = \sum_m B_{2n+1,2m+1} \left(\frac{qc}{a} \right) \sin(2m+1)\xi \quad (59)$$

The function $s e_1$ may be taken from the tables computed by Goldstein, noting that q_G is negative for real values of q (reference 9, p. 304). The functions $s e_3$, $s e_5$, etc., as far as we know, have not yet been computed. Using Goldstein's method, we first computed the values of v and then the coefficients of the Fourier series to obtain the functions $s e_3$ and $s e_5$.⁵⁾ Figures 17, 18, and 19 show the variation of the Fourier coefficients of $s e_1$, $s e_3$, and $s e_5$ with q_G .

We require, in addition, the corresponding Mathieu functions with imaginary arguments. These will be denoted

⁵⁾ The computations were carried out by F. Riegels. In computing the values of v the work of E. L. Ince (reference 10) was used.

by the letters $S_{2n+1}(\eta)$. B. Sieger (reference 11) has shown that between the corresponding functions there exist relations such that

$$S_{2n+1,q}(\eta) = \frac{1}{\pi} \int_0^{2\pi} \frac{q}{8a} I_{2n+1}\left(\frac{q}{a}r\right) \sin(2n+1)\vartheta \cdot s e_{2n+1, \frac{qc}{a}}(\xi) d\xi \quad (60)$$

where

$$\left. \begin{aligned} r \cos \vartheta &= c \cosh \eta \cos \xi \\ r \sin \vartheta &= c \sinh \eta \sin \xi \end{aligned} \right\} \quad (61)$$

and

With the aid of an addition theorem for Bessel functions (reference 12), the integration of (60) may be performed. The theorem is:

$$\frac{I_v(\lambda r)}{\lambda^v r^v} = 2^v \Gamma(v) \sum_{m=0}^{m=\infty} (v+m) \frac{I_{v+m}\left(\frac{\lambda c}{2} e^\eta\right) I_{v+m}\left(\frac{\lambda c}{2} e^{-\eta}\right)}{(-1)^m \left(\frac{\lambda c}{2}\right)^{2v}} C_m^v (-\cos 2\xi) \quad (62)$$

where $\Gamma(v)$ denotes the gamma function and $C_m^v(p)$ the coefficients of a^m in the development of $(1 - 2\alpha p + \alpha^2)^{-v}$ according to increasing powers of α . From equation (60) there results:

$$S_{2n+1,q}(\eta) = \sinh \eta \sum_{m=1}^{m=\infty} b_{2n+1,m}(q) I_m\left(\frac{q}{a} \frac{c}{2} e^\eta\right) I_m\left(\frac{q}{a} \frac{c}{2} e^{-\eta}\right) \quad (63)$$

with

$$b_{2n+1,m} = m [B_{2n+1,1} - B_{2n+1,3} \cdots (-1)^{m+1} B_{2n+1,2m-1}] \quad (64)$$

For the function S_1 , the series is convergent. For higher orders it is often necessary, for values of η that are not too small, to obtain the function directly by integration of (60), since the accurate computation of the higher order Bessel functions $I_m\left(\frac{q}{a} \frac{c}{2} e^\eta\right)$ would take too much

time. We shall limit ourselves in our computations, to the determination of the downwash velocity behind the wing. For this we have the value (see equation 54)):

$$\frac{\partial \Phi}{\partial z} = \frac{\partial \Phi_1}{\partial z} + \frac{1}{c \sin \zeta} \frac{\partial \Phi_2}{\partial \eta} \quad (65)$$

From equation (50), substituting

$$\text{and } M_{v,q}(\zeta) = s e_{2n+1,q}(\zeta) \quad (66)$$

$$\bar{M}_{v,q}(\eta) = S_{2n+1,q}(\eta)$$

there results:

$$\frac{\partial \Phi_2}{\partial z} = - \frac{\Gamma}{4\pi} \sum_n \frac{1}{n} \int_0^\infty \left[\frac{\sin \left(q \frac{\zeta}{a} \right) S'_{2n+1,q}(0)}{q S_{2n+1,q}(\eta_0)} \right] \int_{-\infty}^\infty \{ \cos q \alpha d\alpha$$

$$\frac{1}{\pi} \int_0^{2\pi} F(\alpha, \eta_0, \zeta^*) s e_{2n+1,q}(\zeta^*) d\zeta^* \} s e_{2n+1,q}(\zeta) dq \quad (67)$$

We therefore require to determine only the quotients:

$$m_{2n+1,q} = \frac{S'_{2n+1,q}(0)}{S_{2n+1,q}(\eta_0)} \quad (68)$$

This quotient is plotted in figures 20 and 21 for $n = 0$ and $n = 1$.

In the computation it turned out that the first term of the series in n contributed the essential part. This is due to the fact that for small values of q only the first and third terms are significant in the Mathieu function expansion $s e_{2n+1,q}(\zeta)$.

3. Results. - With a free elliptical jet with $\sqrt{2}$ axis ratio, the downwash velocity due to the jet boundary was determined along the jet axis for the case of a wing of very short span and one whose span was equal to the distance between the foci. It was assumed that the wing had uniform lift distribution. For the finite wing there was, in addition, determined the mean value of the velocity behind the wing:

$$w_k = \frac{\int_{-c}^{+c} \frac{\partial(\Phi_1 + \Phi_2)}{\partial z} dy}{2c} \quad (69)$$

as a function of the distance $l/2a$ from the center of pressure line of the wing (fig. 22).

It is usual to represent the mean downwash velocity in the form:

$$\frac{w_k}{V} = \frac{c_a}{8} \frac{F}{F_0} \delta \quad (70)$$

where c_a is the lift coefficient of the wing, F_0 the cross-sectional area of the tunnel, V the blower velocity, δ a nondimensional coefficient which is a function of the distance l from the center of pressure line of the wing and of the ratio wing span/jet width. Figure 23 shows δ as a function of the ratio wing span/jet width. For comparison, the corresponding values for a circular jet are also indicated. If the coefficient δ in equation (70) is split up by using δ_0 to denote the value of δ at the wing:

$$\frac{w_k}{V} = \frac{c_a}{8} \frac{F}{F_0} \delta_0 (1 + \tau) \quad (71)$$

it turns out that the curves $\tau (l/2a)$ practically coincide for $b = 0$ and $b = c$, so that it may be assumed that τ is nearly independent of the span for one and the same jet section. It is therefore possible to determine the downwash velocities for all spans between 0 and $2c$ from the foregoing computations, provided δ_0 is known. Figure 24 shows τ . For comparison the corresponding values for the circular jet of equal width ($2a = 2r_0$) are also indicated on the figure; in that case, $\delta_0 = 1$. The value of δ_0 for the elliptical jet is known from the computations of Sanuki and Tani (fig. 25).

In order to distinguish the effect of the elliptical cross section on the downwash behind the wing we shall compare with a circular jet of equal cross-sectional area. For a wing of very small span we may obtain the value δ of the elliptical jet approximately by taking the value for a circular jet of equal area and considering that $\delta(0)$

is not equal to 1 but is δ_0 . Figure 26 gives the result and shows that the approximation is good, which result may be expected when the eccentricity of the ellipse is not too large.

In measuring the moments of the wing it is of interest to know the distribution of the downwash along the span. Figure 27 shows the variation of the downwash along the wing span having uniform lift distribution.

III. Induced Velocity in Closed Tunnel

1. Theoretical considerations.— In an infinite flow the airfoil would induce at the surface of the elliptic cylinder, which corresponds to the tunnel boundary, the normal velocity v_{n_0} . Since the normal velocities at the

cylinder surface must vanish at the boundary, as the air can flow only along the wall, we must superimpose a velocity field which has a normal velocity component $-v_{n_0}$ at the surface. We proceed in the same way as was done for the elliptical free jet. We first superimpose on the potential field of the wing Φ_0 a field Φ_1 which is produced by the so-called "vortex images" and which assures that the boundary conditions are satisfied at infinity. The position of these vortex images is the same as for the free jet but the sense of rotation is partly different. To determine the latter we consider a section through the tunnel at an infinite distance behind the wing (fig. 28). The vortices outside the ellipse must, together with the vortex pair within the ellipse, induce on the boundary a velocity which is always in the direction of the tangent to the ellipse; that is, which has no component normal to the boundary. We may see these relations clearer if we transform the ellipse into a rectangle (fig. 29). The curved boundary of the ellipse then goes over into the straight line $C''\bar{C}'$. The flow must now take place along this straight wall. It may be seen that, contrary to what was the case for the free jet, the sense of rotation must change along the horizontal lines but remains the same along the vertical lines. Figure 30 shows the position of the vortex images in the xyz system of coordinates for the case where the span is equal to the distance between the foci $2c$.⁵⁾ The sense of rotation is indicated. For

⁵⁾ In this case the point P_1^* in figure 29 moves to the origin.

spans $2b < 2c$ and $2b = 0$, the corresponding figures may easily be obtained by comparing with figures 15 and 16.

The potential $(\Phi_0 + \Phi_1)$ satisfies the boundary condition at infinity. To reduce the remaining velocities $(v_{n_0} + v_{n_1})$ to zero it is still necessary to superimpose another potential Φ_2 , which is determined by the condition that the equation

$$\frac{\partial \Phi_2}{\partial n} = - \left(\frac{\partial \Phi_0}{\partial n} + \frac{\partial \Phi_1}{\partial n} \right) = - (v_{n_0} + v_{n_1}) \quad (72)$$

holds true at the cylinder surface. For the potential we obtain in a similar way as for the free jet:

$$\begin{aligned} (\xi, \eta, \zeta) &= \frac{\Gamma}{4\pi} \sum_{\nu} \frac{1}{\pi} \int_0^\infty \left[\frac{\sin \left(q \frac{\xi}{a} \right)}{\left(\frac{\partial M_{\nu, q}(\eta)}{\partial \eta} \right)} \right]_{-\infty}^{+\infty} \left\{ \sin q \alpha d\alpha \right. \\ &\quad \left. \frac{1}{\pi} \int_0^{2\pi} F^*(\alpha, \eta_0, \zeta^*) M_{\nu, q}(\zeta^*) d\zeta^* \right\} \\ &\quad M_{\nu, q}(\zeta) M_{\nu, q}(\eta) dq \end{aligned} \quad (73)$$

where ξ, η, ζ denote elliptic coordinates. On the cylinder surface $\eta = \text{constant} = \eta_0$. The coordinates ξ and ζ appear in the inner integrals as variables of integration. To avoid confusion the integration variable is replaced by ζ^* and ξ/a by α . $M_{\nu, q}(\zeta)$ and $M_{\nu, q}(\eta)$ denote the Mathieu functions with real and variable arguments which satisfy the differential equations (51) and (52). The function $F^*(\alpha, \eta_0, \zeta^*)$ is connected with $(v_{n_0} + v_{n_1})$ by the relation:

$$F^*(\alpha, \eta_0, \zeta^*) = \frac{-(v_{n_0} + v_{n_1})}{\frac{\Gamma}{4\pi a}} \frac{c}{a} \sqrt{\cosh^2 \eta_0 - \cos^2 \zeta^*} \quad (74)$$

If the components v_y and v_z of the sum are introduced in place of the sum, there results:

$$F^*(\alpha, \eta_0, \zeta^*) = -\frac{1}{\Gamma} \frac{c}{a} \left\{ v_y \sinh \eta_0 \cos \zeta^* + v_z \cosh \eta_0 \sin \zeta^* \right\} \quad (75)$$

The induced velocity we are seeking is, in general, given by equation (53), for points in the xy plane by equations (54) and (55). We shall limit ourselves to the case where the span of the wing does not exceed the distance

between the foci. We then require $\frac{\partial \Phi_2}{\partial \eta}$. For this purpose the value of $\frac{\partial \Phi_2}{\partial \eta}$ for $\eta = 0$ shall be specified and out of the solutions of the Mathieu differential equation, those suited to this problem chosen and substituted:

$$\begin{aligned} \left(\frac{\partial \Phi_2}{\partial \eta} \right) &= \frac{\Gamma}{4\pi} \sum_n \frac{1}{n} \int_0^\infty \frac{S'_{2n+1,q}(0)}{S'_{2n+1,q}(\eta_0)} \sin \left(q \frac{\xi}{a} \right) \int_{-\infty}^{+\infty} [\sin q \alpha \, d\alpha \\ &\quad \frac{1}{\pi} \int_0^{2\pi} F^*(\alpha, \eta_0, \zeta^*) s e_{2n+1,q}(\zeta^*) \, d\zeta^*] \\ &\quad s e_{2n+1,q}(\xi) \} \, dq \end{aligned} \quad (76)$$

The quotient

$$\bar{m}_{2n+1,q} = \frac{S'_{2n+1,q}(0)}{S'_{2n+1,q}(\eta_0)}$$

for $n = 0$ is shown on figure 31 plotted for the case where the axis ratio is $\sqrt{2}$.

2. Results⁶⁾. - A jet section was chosen whose axis ratio was $a/b_1 = \sqrt{2}$. The induced velocity along the tunnel axis was determined for two cases, namely:

- 1) Wing span equal to distance between foci.
- 2) Very small wing spans.

The lift distribution was uniform. For the wing of finite span, there was, in addition, determined the mean velocity behind the wing as a function of the distance $l/2a$ from the center of pressure line of the wing (fig. 32). The downwash velocity for the closed tunnel is negative, that

⁶⁾ The computations were actually carried out by F. Riegels, for whose assistance I take this opportunity to express my thanks.

is, it is really an upwash velocity, which leads to an increase in the angle of attack of the wing. For a given lift in a closed wind tunnel the angle of attack measured is therefore too small.

The mean downwash velocity in a closed tunnel may again be given in the form:

$$\frac{w_k^*}{V} = - \frac{c_a}{8} \frac{F}{F_0} \delta \quad (78)$$

Figure 33 shows δ as a function of the ratio wing span/jet width. For comparison the value of δ for a circular jet of equal width is also indicated.

If in equation (78) the coefficient δ is split up, denoting its value at the wing by δ_0 ,

$$\frac{w_k^*}{V} = - \frac{c_a}{8} \frac{F}{F_0} \delta_0 (1 + \tau^*) \quad (79)$$

the result is, as in the case of the free jet, that the curves τ^* ($l/2a$) for $b = 0$ and $b = 2c$ run so close to each other that for all practical purposes τ^* may be assumed independent of the span for one and the same cross section. This means that in this case too it is possible to obtain the downwash velocity for all spans between 0 and $2c$ provided only δ_0 is known. Figure 34 shows τ^* ; for comparison, the corresponding value for a circular section of equal width is also shown. The correction factor δ_0 for uniform lift distribution was computed by Sanuki and Tani (reference 3); it is shown in figure 35 as a function of the ratio wing span/tunnel width.

At the distance l behind the wing the induced velocity produced by the tunnel boundary is greater than at the wing itself. A horizontal tail surface at that position therefore has a different effect on the pitching moment, at a given angle of attack, than it would have in free flight. In the closed tunnel the effective angle of attack is increased in the ratio

$$\frac{\Delta w_k^*}{V} = \frac{c_a}{8} \frac{F}{F_0} \delta_0 \tau^* \quad (80)$$

REFERENCES

1. Seiferth, R., and Betz, A.: Untersuchung von Flugzeugmodellen im Windkanal, Handbuch der Experimentalphysik, vol. 4, part 2, pp. 166-69.
2. Glauert, H.: Wind Tunnel Interference on Wings, Bodies, and Airscrews. R. & M. No. 1566, British A.R.C., 1933.
3. Sanuki and Tani: The Wall Interference of a Wind Tunnel of Elliptic Cross-Section. Proc. Phys. Math. Soc. Jap. III. Ser., vol. 14 (1932), pp. 592-603.
4. Rosenhead: The Aerofoil in a Wind Tunnel of Elliptic Section. Proc. Roy. Soc., London. A 140 (1933), pp. 579-604.
5. Burgers, J. M., in "Aerodynamic Theory by W. F. Durand.", vol. 2. Verlag J. Springer, Berlin, 1935.
6. Cowley, W. L., and McMillan, G. A.: Effect of Wind Tunnel Wall Interference on the Pitching Moments of Large Models in the Duplex Tunnel. R. & M. No. 1639, British A.R.C., 1935.
7. Knight, M., and Harris, T. A.: Experimental Determination of Jet Boundary Corrections for Airfoil Tests in Four Open Wind Tunnel Jets of Different Shapes. T.R. No. 361, N.A.C.A., 1930.
8. Strutt, M. J. O.: Lamesche und Mathieusche und verwandte Funktionen in Physik und Technik, Ergebnisse der Mathematik und ihrer Grenzgebiete, Verlag J. Springer, Berlin, 1932.
9. Goldstein, S.: Mathieu Functions. Trans. Philos. Soc. Cambridge, vol. 23, no. 11, pp. 303-36.
10. Ince, E. L.: Researches into the Characteristic Numbers of the Mathieu Equation. (Second Paper), Proc. Roy. Soc. Edinburgh (1925-26), p. 316.
11. Sieger, B.: Die Beugung einer ebenen elektrischen Welle an einem Schirm von elliptischem Querschnitt. Diss. Würzburg 1908. Ann. Physik IV. Folge, vol. 27, (1908).
12. Watson, G. M.: A Treatise on the Theory of Bessel Functions. Cambridge 1922, p. 365.

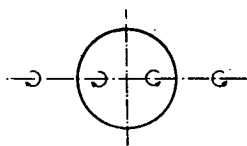


Figure 1.- Vortex images for the open circular jet.

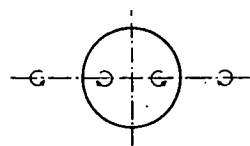


Figure 2.- Vortex images for the closed circular tunnel.

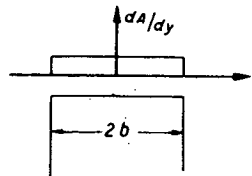


Figure 3.- Wing with uniform lift distribution (horse-shoe vortex)

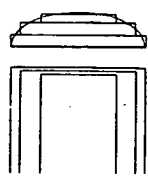


Figure 4.- An airfoil built up of horseshoe vortices.

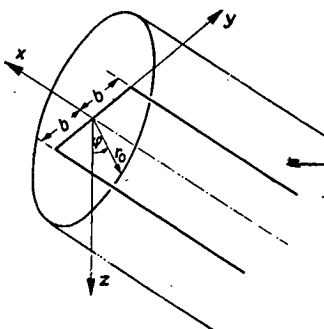


Figure 5.- System of coordinates

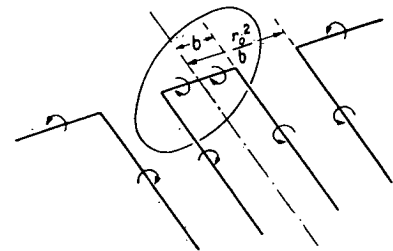


Figure 6.- Images of horseshoe vortex at the boundary of the free jet

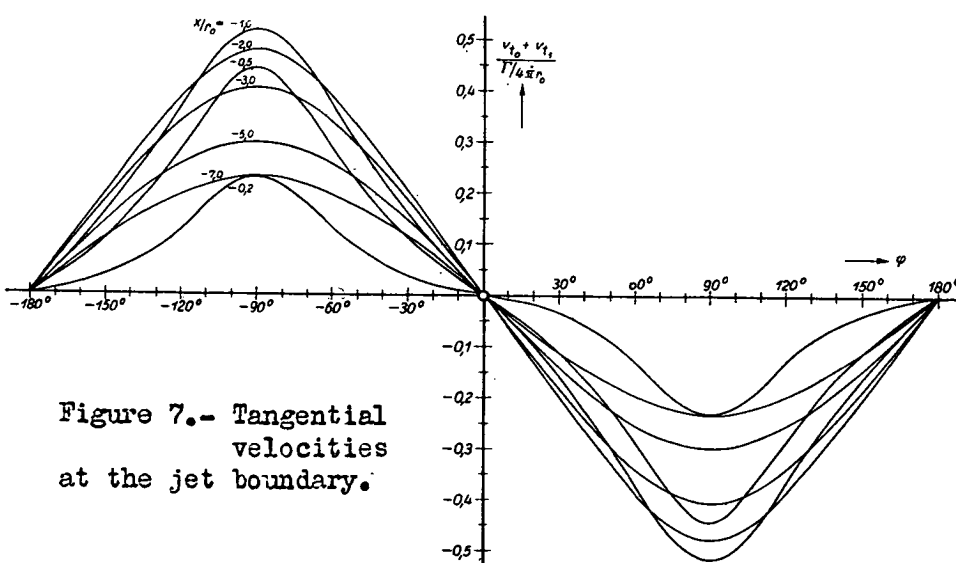
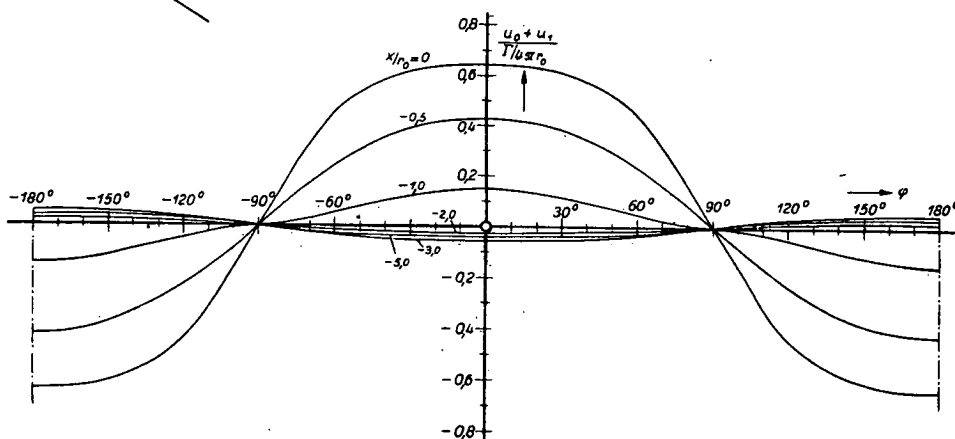


Figure 7.- Tangential velocities at the jet boundary.

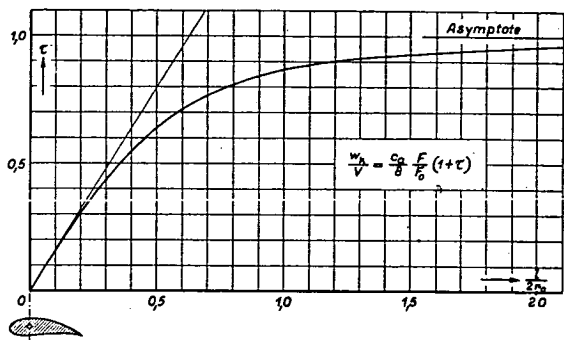


Figure 8.- Value of τ along the free jet axis.

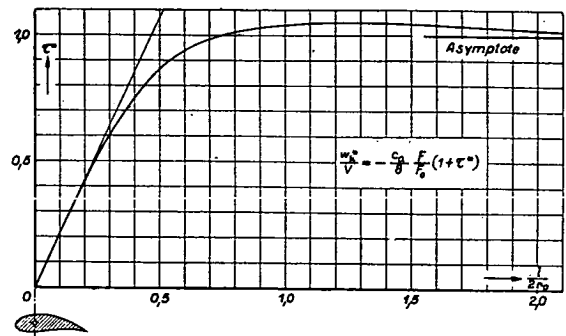


Figure 9.- Value of τ^* along jet axis in closed tunnel.

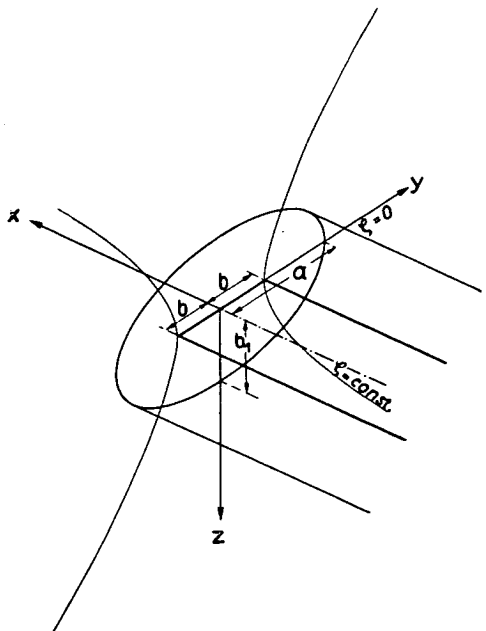


Figure 10.- Coordinate system.

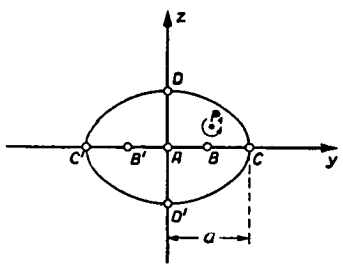


Figure 12.

Figures 12 and 13.- Transformation of ellipse into rectangle.

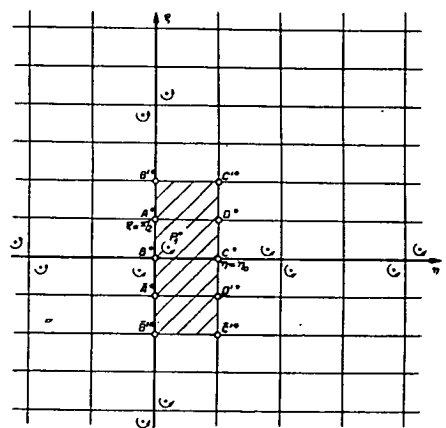


Figure 13.

Figure 14.- Images of horseshoe vortex at the elliptical jet boundary. Span greater than or equal to the distance between foci.

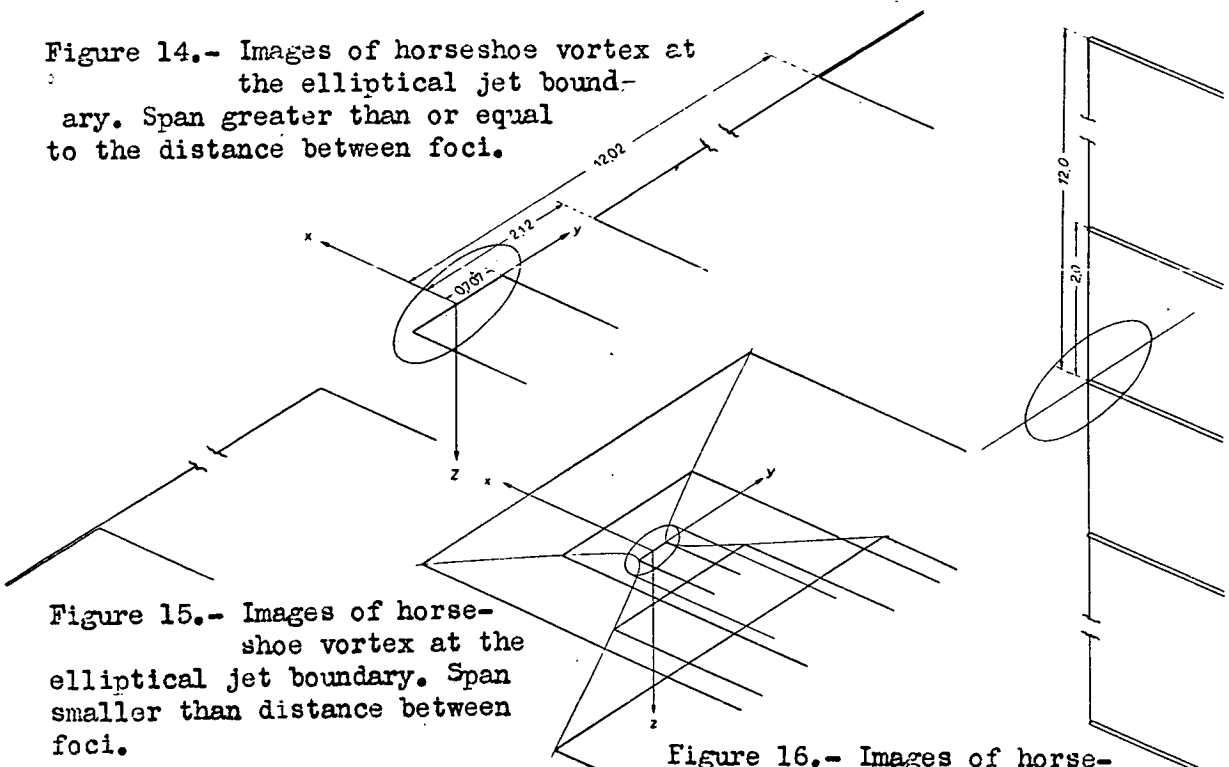


Figure 15.- Images of horseshoe vortex at the elliptical jet boundary. Span smaller than distance between foci.

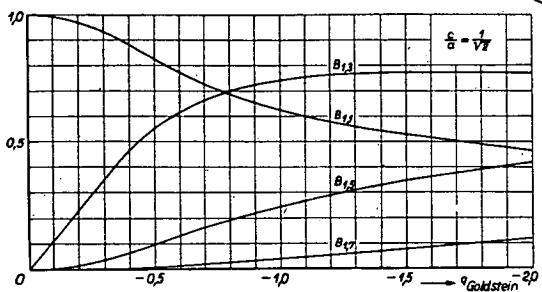


Figure 17.

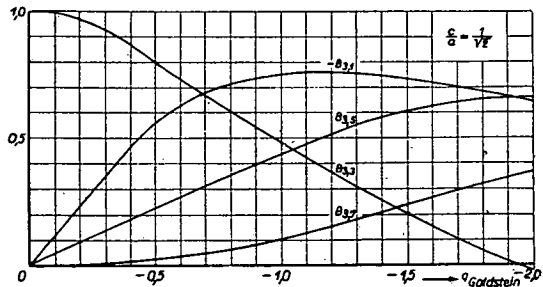
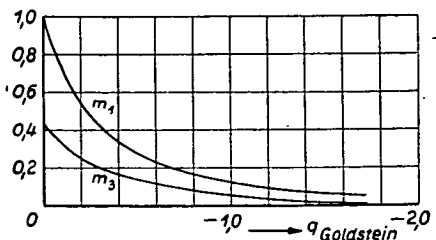
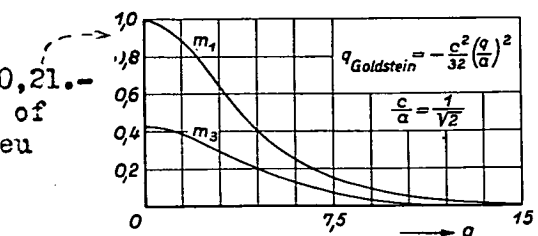


Figure 18.



Figures 20,21.- Quotients of the Mathieu function.



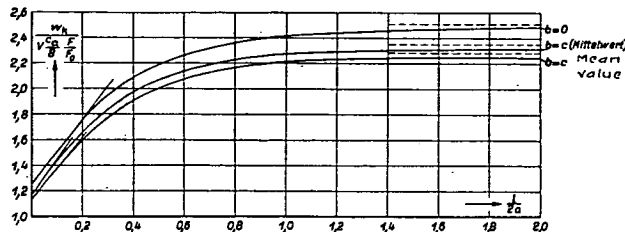


Figure 22.- Downwash behind airfoil in elliptic free jet.

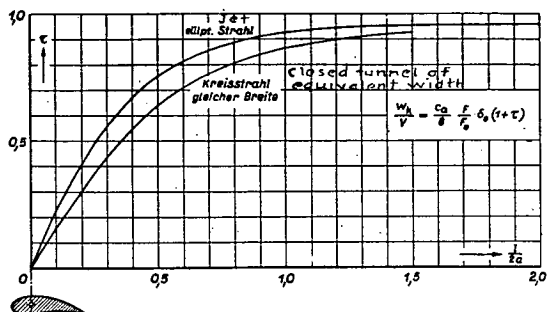


Figure 24.- For the computation of the mean value of the downwash w_k/V behind an airfoil in an elliptic jet ($l/2a$ = distance from pressure line wing)

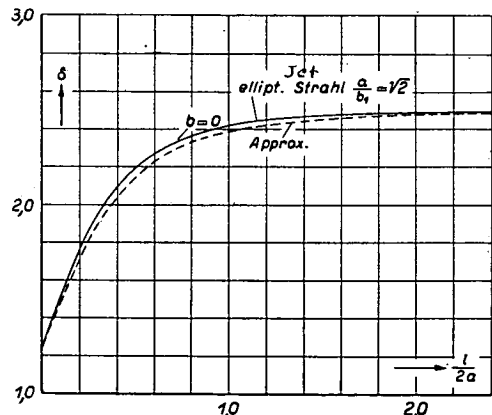


Figure 26.- Effect of shape of jet.

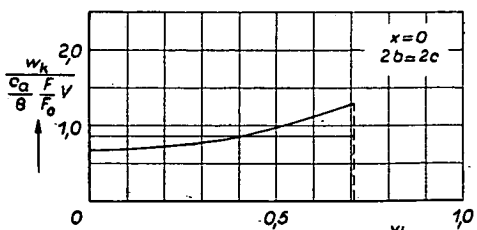


Figure 27.- Distribution of downwash along wing span.

Figs. 22,23,24,25,26,27,31,32

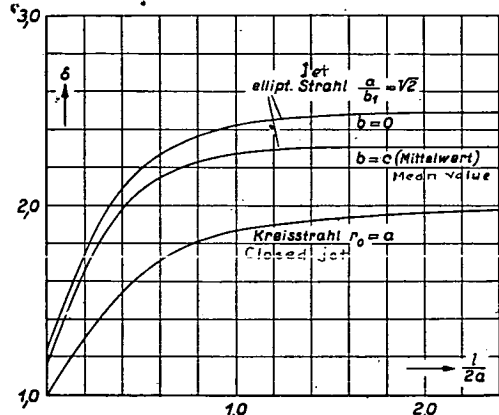


Figure 23.-Variation of the factor δ with ratio wing span/jet width and with shape of cross section.

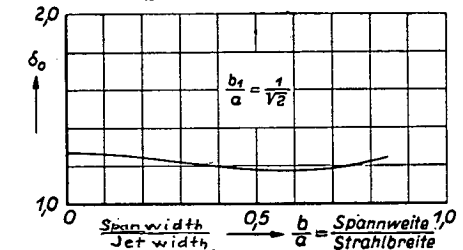


Figure 25.- Correction factor δ_0 for the computation of the downwash at the wing in elliptic free jet.

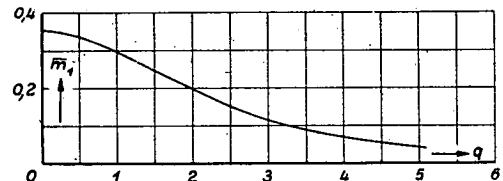


Figure 31.- Quotient of the Mathieu function \bar{m}_1 plotted against q .

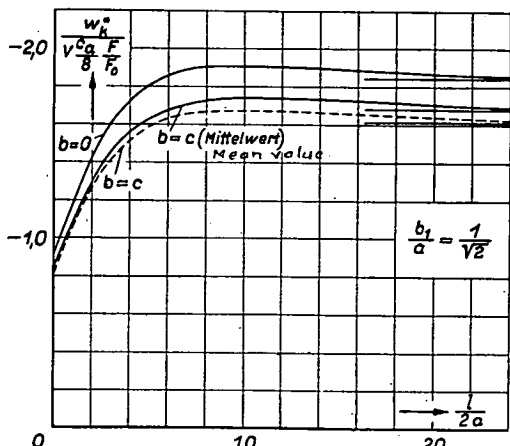


Figure 32.-"Downwash" behind airfoil in closed elliptical tunnel.

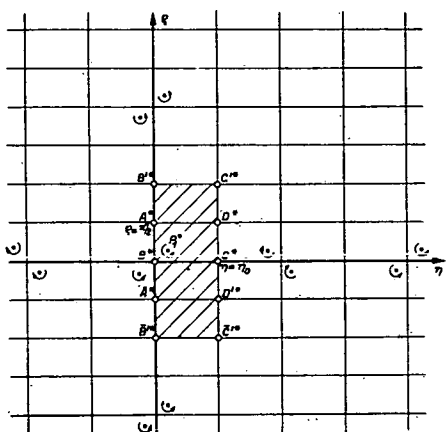


Figure 29

Figures 28,29.-

Transformation of ellipse into rectangle. Images formation in closed tunnel.

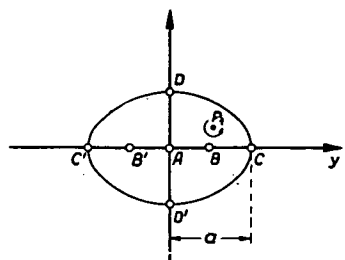


Figure 28

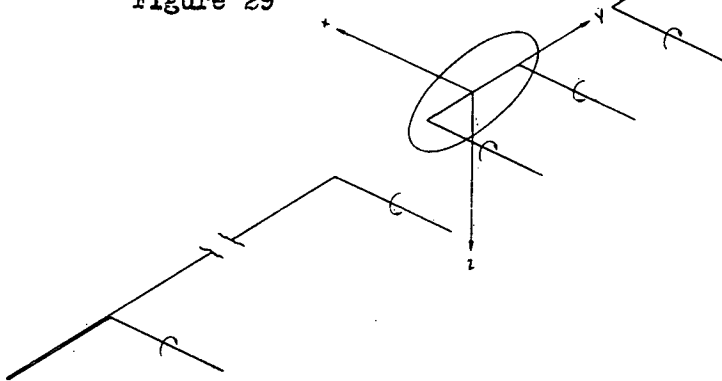


Figure 30.- Images of horseshoe vortex at the boundary of the closed tunnel of elliptic cross section. Span equal to distance between foci.

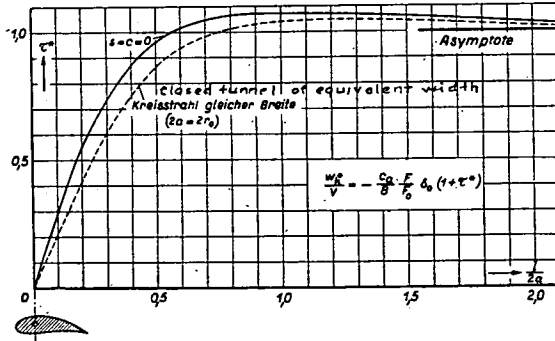


Figure 34.- For computing the mean value of the "downwash" w_k/V behind an airfoil in closed tunnel of elliptic cross section ($l/2a =$ distance from pressure line of wing).

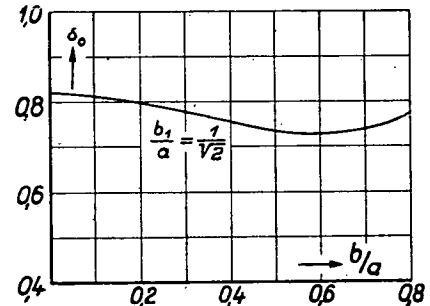


Figure 35.- Correction factor δ_0 for computation of "downwash" at the wing in closed elliptic tunnel.

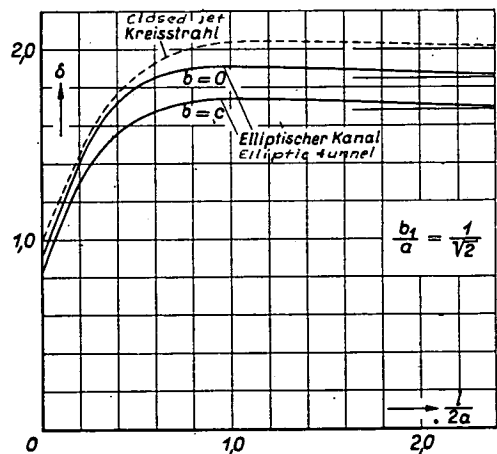


Figure 33.- Variation of factor δ with ratio wing span/width of jet and with shape of jet section.